Original Article

Comparison of silent MRA and time-of-flight MRA in the depiction and grading of brain arteriovenous malformations

Chunxue Wu[1,2#], Mengqi Dong[3#], Zhenxiang Zang[1,2], Yi Shan[1,2], Jiaxing Yu[3], Tao Hong[3], Kun Yang[4], Cheng Zhao[1,2], Hongqi Zhang[3*], Jie Lu[1,2*]

[1]Department of Radiology and Nuclear Medicine, Xuanwu Hospital, Capital Medical University, Beijing, China; [2]Beijing Key Laboratory of Magnetic Resonance Imaging and Brain Informatics, Beijing, China; [3]Department of Neurosurgery, Xuanwu Hospital, Capital Medical University, Beijing, China; [4]The Office of National Center for Neurological Disorders, Xuanwu Hospital, Capital Medical University, Beijing, China

Contributions: (I) Conception and design: C Wu, M Dong, J Lu, H Zhang; (II) Administrative support: J Lu, H Zhang; (III) Provision of study materials or patients: C Wu, M Dong, J Yu, T Hong; (IV) Collection and assembly of data: C Wu, M Dong, Z Zang, C Zhao; (V) Data analysis and interpretation: C Wu, M Dong, Z Zang, Y Shan, K Yang; (VI) Manuscript writing: All authors; (VII) Final approval of manuscript: All authors.

[#]These authors contributed equally to this work as co-first authors.

[*]These authors contributed equally to this work.

Correspondence to: Jie Lu, MD. Department of Radiology and Nuclear Medicine, Xuanwu Hospital, Capital Medical University, Beijing, China; Beijing Key Laboratory of Magnetic Resonance Imaging and Brain Informatics, 45# Changchun Street, Xicheng District, Beijing 100053, China. Email: imaginglu@hotmail.com; Hongqi Zhang, MD. Department of Neurosurgery, Xuanwu Hospital, Capital Medical University, 45# Changchun Street, Xicheng District, Beijing 100053, China. Email: xwzhanghq@163.com.

Background: Preliminary small-sample studies suggest that silent magnetic resonance angiography (MRA) has an advantage over time-of-flight MRA (TOF MRA) in the characterization of brain arteriovenous malformation (BAVM), but did not examine whether the imaging performance of silent MRA was affected by the intrinsic features of BAVM or common clinical factors. This study sought to compare silent MRA and TOF MRA in terms of the visualization and grading of BAVMs in various clinical settings.

Methods: In total, 85 participants (50 males, 35 females; mean age: 33.5±15.2 years) with BAVM who underwent both silent MRA and TOF MRA using a 3 Tesla (3T) magnetic resonance imaging (MRI) system were consecutively recruited from the Capital Medical University Xuanwu Hospital between April 2020 and October 2022 to participate in this cross-sectional retrospective study. The patients were divided into subgroups according to new hemorrhage presentation, embolization, size, and nidus compactness. Image quality scoring on a 4-point scale, and the accuracy of characteristic visulization and Spetzler-Martin grading were compared between the two MRA techniques and each MRA subgroup using the rank-sum Wilcoxon test and Fisher's exact test with digital subtraction angiography (DSA) as the reference standard. A multivariable chi-square test was used to examine the interactions between the grouping factors. A P value <0.05 was considered statistically significant.

Results: The average image quality scores were significantly higher for silent MRA than those for TOF MRA overall (2.83±0.42 versus 2.46±0.66, P<0.001) and in each subgroup (P<0.05). For silent MRA, the average image quality score for BAVM in each subgroup did not differ significantly (P>0.05). For TOF MRA, the image quality scores for the new hemorrhage, small nidus, and diffuse nidus groups was significantly reduced (P=0.001, <0.001, and 0.037, respectively). The accuracy of silent MRA was significantly better than that of TOF MRA in terms of nidus size and Spetzler-Martin grading (P<0.001), but did not differ significantly in terms of deep venous drainage and associated aneurysm (P=0.402, 0.098, respectively). In relation to silent MRA, the image quality, detection of BAVM characteristics, and grading were similar across

the new hemorrhage, embolization, size, and compactness subgroups (P=0.066–0.959). In relation to TOF MRA, the accuracy of nidus size grading was significantly lower in the medium-size subgroup than the small-size subgroup (P<0.001).

Conclusions: Silent MRA performed well in imaging BAVM, and high performance in determining nidus size and Spetzler-Martin grading, but its ability to detect deep venous drainage was limited.

Keywords: Brain arteriovenous malformation (BAVM); silent magnetic resonance angiography (silent MRA); time-of-flight magnetic resonance angiography (TOF MRA); Spetzler-Martin grading; hemorrhage

Submitted Jun 04, 2024. Accepted for publication Oct 23, 2024. Published online Nov 29, 2024.
doi: 10.21037/qims-24-1097
View this article at: https://dx.doi.org/10.21037/qims-24-1097

Introduction

Brain arteriovenous malformation (BAVM) is a complex abnormal arteriovenous shunt in which arteries and veins connect directly at the vessel nidus without a normal intervening capillary bed (1,2). Challenges in the treatment of BAVM include the risk of hemorrhage in the natural history of the disease, and the risk associated with the intervention itself (3-6). The risk of hemorrhage is closely related to some of the characteristics of BAVM, such as the small nidus size, deep draining veins, or associated aneurysms (7-9). In addition, the Spetzler-Martin grading scale, which is the most commonly used method for predicting outcomes after microsurgery, is also based on specific angioarchitecture. Thus, imaging techniques that can reliably display the angioarchitecture characteristics of BAVM need to be developed.

Digital subtraction angiography (DSA) is the gold standard for the characterization and grading of BAVMs (10). However, DSA is an invasive examination that carries the risk of procedure-related complications, and is thus not suitable for serial imaging follow-ups (11-13). In clinical practice, three-dimensional (3D) time-of-flight magnetic resonance angiography (TOF MRA) with multiple overlapping thin slabs is most frequently performed to identify BAVM. This technique does not require a contrast injection and can depict some anatomic details of BAVM well, but it is constrained by the saturation of spins in slow, complex, or in-plane flow, and only offers a limited amount of information about BAVM (14).

Based on pseudo-continuous arterial spin labeling (ASL) and zero-time echo (zTE) technology (15), silent magnetic resonance angiography (MRA) is a new imaging method that does not use radiation or require a contrast agent (16-18). Preliminary studies suggest that silent MRA has advantages over TOF MRA in depicting BAVM (19-21). However, these studies had small sample sizes and did not examine the performance of silent MRA in evaluating the angioarchitecture characteristics of BAVM or whether its imaging performance is affected by the intrinsic characteristics of BAVM or other common clinical factors (e.g., hemorrhage and embolization), limiting the wide application of silent MRA in clinical settings. Therefore, it is necessary to conduct a more thorough investigation of this technique's performance in different clinical situations and limitations in displaying BAVM's angioarchitecture and grading to determine whether it could aid in the accurate diagnosis of BAVM and subsequent treatment decisions.

This study sought to assess the performance of silent MRA in the characterization and Spetzler-Martin grading of BAVMs compared to TOF MRA. We present this article in accordance with the STROBE reporting checklist (available at https://qims.amegroups.com/article/view/10.21037/qims-24-1097/rc).

Methods

The study was conducted in accordance with the Declaration of Helsinki (as revised in 2013). This study was approved by the Ethics Committee of Xuanwu Hospital of Capital Medical University (Xuanwu Hospital, No. 2022079). Informed consent was obtained from all adult patients. For patients under 18 years old, consent was obtained from their parents or legal guardians.

Patients

In total, 98 consecutive patients with BAVM diagnosed by DSA were examined between April 2020 and October

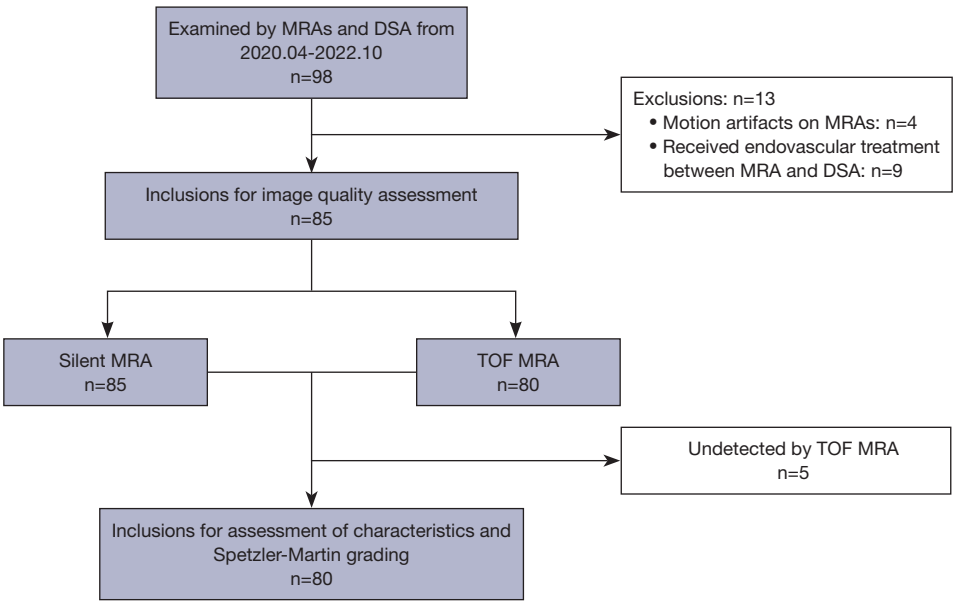

Figure 1 Flow chart illustrating patient selection process. MRA, magnetic resonance angiography; DSA, digital subtraction angiography; TOF, time-of-flight.

2022 using both TOF MRA and silent MRA. Patients were excluded from the study if they met any of the following exclusion criteria: (I) had undergone the MRA and DSA examinations more than two weeks apart; (II) had received microsurgery, endovascular treatment, or radiotherapy between the MRI and DSA examinations; and/or (III) had poor-quality images due to motion artifacts. Of the 98 consecutive patients, 13 were excluded from the study because they received endovascular treatment between MRA and DSA, or had motion artifacts on their MRA images. Ultimately, 85 patients were included in the study (of whom 35 were female and 50 were male). The patients had a mean age of 33.5±15.2 years (range, 5–64 years). The mean period between the DSA and MRA examinations was 4±2.2 days (range, 0–7 days; median: 1 day). Image quality was assessed for all the 85 patients with BAVM. The angioarchitecture characteristic evaluation and Spetzler-Martin grading evaluation were performed on BAVMs that can be detected by both MRA techniques. A flow chart illustrating the patient selection process is shown in *Figure 1*.

MRI protocols

The conventional MRI, silent MRA, and TOF MRA examinations were performed during the same scan session using a 3 Tesla (3T) system (Signa; GE Healthcare, Milwaukee, WI, USA) with a 48-channel head coil. The conventional magnetic resonance imaging (MRI) protocol included axial T2-weighted image (T2WI), and 3D sagittal T1 Magnetization-Prepared Rapid Acquisition Gradient Echo (T1 MPRAGE). The TOF MRA parameters were as follows: repetition time (TR): 25 ms; echo time (TE): 2.9 ms; slice thickness: 1.2 mm; slabs: 4; NEX: 1; bandwidth: 41.67 kHz; field of view (FOV): 20 cm × 20 cm; flip angle: 15°; and total acquisition time: 6:21 min. The silent MRA parameters were as follows: TR: 828 ms; TE: 0 ms; slice thickness: 1.2 mm; NEX: 1; bandwidth: 25 kHz; FOV: 20 × 20 cm; matrix: 150 × 150; flip angle: 5°; total acquisition time: 6 min 59 s; and labeling duration: 2,034 ms. 3D radial sampling was applied during the readout scheme. To avoid the influence of the labeled position on the results, the lower edge of the FOV was located at the lower edge of the C2 vertebral body level in each patient (22).

Conventional angiography

DSA was conducted using a biplane system (Integris V5000; Philips Medical Systems). Frontal and lateral views with a frame rate of four per second were displayed. DSA was performed by one neurosurgeon (P.H., with 10 years of experience) who was not involved in reading either the MRA or DSA images.

Grouping criteria

All BAVMs were allocated to several subgroups based on the presence of a new hemorrhage, a history of embolization, and the size and compactness of the nidus. A new hemorrhage was defined as hyperintensity on T1WI that was consistent with the patient's clinical presentation (10). The largest diameter of the nidus in three dimensions was measured using DSA to determine its size (10). Nidus dimensions were categorized as tiny (<3 cm), medium (3–6 cm), or large (>6 cm). A BAVM was classified as compact if the margins were clear, or diffuse if the margins were unraveled and/or the T2WI axial view showed brain parenchyma interspersed with the nidus (23).

Image analysis

The silent MRA and TOF MRA images were reviewed independently by one neuroradiologist (C.W., with 12 years of experience) and one neurosurgeon (M.D., with 8 years of experience) using maximum intensity projection (MIP) views in random order on a GE Healthcare Advantage Workstation 4.7 (GE Healthcare). The two readers were blinded to the patients' histories and DSA results. Each reader reviewed the silent MRA and TOF MRA images separately. The reading interval of the two MRA sequences was 2 weeks to avoid recall bias.

For each BAVM component (i.e., the arterial feeders, nidus, and venous drainage), the MRA image quality was rated as follows—3: excellent for diagnosis (clearly detected continuously to the nidus with clearly detailed vascular architecture); 2: adequate for diagnosis (not necessarily clear or minor artifacts were present but did not interfere with detailed vascular architecture); 1: doubtful for diagnosis (poor imaging quality with a poor depiction of the vascular architecture, but detectable); and 0: non-diagnostic (undetectable) (12). Disagreements were resolved by discussion to establish consensus. The overall score for image quality in each case was the average of the component scores.

The following characteristics of BAVM were evaluated: the size of the nidus; the presence of deep venous drainage; and associated aneurysms. DSA was used as the reference standard for the characteristics, and was reviewed in a randomized order by one neurosurgeon (J.Y.; with 10 years of experience), who was unaware of the MRA results. For both MRA techniques, the size of the nidus in three dimensions was determined on the basis of the MIP views in lateral and anteroposterior projections. The largest diameter was recorded as the BAVM size (10). Venous drainage was categorized as any deep venous drainage (exclusively deep venous drainage, or superficial and deep venous drainage) or superficial venous drainage. Associated aneurysms were classified as intranidal aneurysms and flow-related aneurysms located on the feeding arteries (22).

Using the Spetzler-Martin grading system (6), the evaluation of the eloquence of the adjacent brain was made by another neuroradiologist (Z.Z.; with 8 years of experience) according to axial T2WI and sagittal T1 MPRAGE of all patients. Finaly, Spetzler-Martin grading was performed for the two MRA techniques and DSA.

Statistical analysis

All the statistical analyses were performed using the Statistical Package for the Social Sciences version 25.0 (SPSS Inc., Chicago, IL, USA). A two-sided P value <0.05 was considered statistically significant. The categorical variables are presented as the percentage. The Shapiro-Wilk test was used to determine whether the continuous variables were normally distributed. The normally distributed continuous variables are presented as the mean with the standard deviation (SD), and the non-normally distributed variables are presented as the median with the range. The rank-sum Wilcoxon test was used to compare the image quality scores and the assessment of BAVM characteristics between silent MRA and TOF MRA, as well as between MRA subgroups. The weighted kappa value of concordance was computed to evaluate interobserver agreement for the image quality score ($\kappa<0.2$: poor; $0.21<\kappa<0.40$: fair; $0.41<\kappa<0.60$: moderate; $0.61<\kappa<0.80$: good; $0.81<\kappa<0.90$: very good; and $\kappa>0.90$: excellent). Fisher's exact test was used to compare the accuracy between silent MRA and TOF MRA in the characterization and Spetzler-Martin grading of BAVMs. The multivariable chi-square test was used to examine the interactions between the grouping factors. Bonferroni correction was used for multiple-comparisons.

Results

Basic characteristics of patients and BAVMs

Of the 85 patients included in the study, 50 (58.8%) patients with BAVM were untreated, and 35 (41.2%) had received embolization before being referred to Capital

Table 1 Distribution of demographic and related BAVM characteristics of patients

Characteristics	Total (n=85)	Grade I (n=17)	Grade II (n=15)	Grade III (n=34)	Grade IV (n=14)	Grade V (n=5)
Demographic						
Male	50	9	9	18	11	3
Median age in years [range]	33.5 [5–64]	25.6 [13–49]	35.9 [14–59]	36.7 [10–63]	32.6 [14–54]	26.8 [5–66]
Preoperative embolization	35	8	7	13	5	2
BAVM						
New hemorrhage	22	9	3	4	6	0
Eloquence	47	0	5	24	13	5
Size <3 cm	26	17	6	3	0	0
Size 3–6 cm	50	0	9	30	11	0
Size >6 cm	9	0	0	1	3	5
Diffuse nidus	15	1	3	5	2	4
Deep drainage	30	0	2	11	12	5
Associated aneurysm	18	3	1	10	4	0

BAVM, brain arteriovenous malformation.

University Xuanwu Hospital, Beijing, China. Forty patients (47.1%) had evidence of hemorrhage on MRI, of whom 22 (25.9%) had a new hemorrhage. Of the patients with partial embolization, nine were treated with onyx and 26 with Glubran-2 as the embolizing agent. A total of 85 nidi were detected on DSA. The average diameter of the nidus was 41.4±22.8 mm (SD). Diffuse nidi were found in 15 patients. The presence of deep venous drainage was observed in 30 patients (35.3%). Eighteen patients had associated aneurysms (21.2%), of which 9 were intranidal aneurysms. There were 17 lesions of grade I, 15 of grade II, 34 of grade III, 14 of grade IV, and 5 of grade V in all BAVMs. The basic characteristics of the patients and BAVMs are summarized in *Table 1*.

Image quality

Of the 85 BAVMs, 83 (97.6%) were detected on silent MRA. TOF MRA detected 80 cases (94.1%), all of which can be seen on silent MRA (*Figure 1*). In the evaluation of the image quality of the arterial feeders, nidus, and venous drainage of BAVMs on silent MRA (κ=0.96, 0.82, and 0.67, respectively, P<0.001) and TOF MRA (κ=0.98, 0.59, and 0.51, respectively, P=0.002) the interobserver agreement was fair to substantial.

The average image quality score for silent MRA was significantly higher than that for TOF MRA (2.83±0.42 *vs.* 2.46±0.66, P<0.001). The image quality of silent MRA was superior to that of TOF MRA in depicting nidi (2.84±0.49 *vs.* 2.21±0.82, P<0.001), venous drainage (2.74±0.58 *vs.* 2.38±0.77, P<0.001), and arterial feeders (2.94±0.33 *vs.* 2.78±0.68, P=0.006). The results of the subgroup assessment of image quality based on new hemorrhage, embolization, nidus size, and morphology are shown in *Table 2*. In terms of image quality, silent MRA was superior to TOF MRA in all subgroups. For silent MRA, the average image quality score for BAVM in each subgroup did not differ significantly (P>0.05). There was no interaction between the subgroup variables. For TOF MRA, the image quality for the new hemorrhage, small nidus, and diffuse nidus groups were significantly reduced (P=0.001, <0.001, and 0.037, respectively) (*Figures 2-4*). There was a significant interaction effect between the new hemorrhage and grading of nidus size subgroups (P=0.031). The image quality score was lower for small nidus in the new hemorrhage group (P<0.001), while the image quality score was independent of the nidus size in the non-new hemorrhage group (P=0.052).

Characterization and grading of BAVMs

In the 80 BAVMs detected by both silent MRA and TOF MRA, the nidus size grading was significantly lower on

Table 2 Subgroup assessment of average score of image quality on silent MRA and TOF MRA

Subgroup grading criteria	Silent MRA	TOF MRA	P value
Total (n=85)	2.83±0.42	2.46±0.66	<0.001*
New hemorrhage			
+ (n=22)	2.77±0.35	2.16±0.68	<0.001*
– (n=63)	2.85±0.36	2.55±0.46	<0.001*
P value	0.542	0.001*	
Embolization			
+ (n=35)	2.81±0.41	2.39±0.57	<0.001*
– (n=50)	2.85±0.32	2.50±0.52	<0.001*
P value	0.606	0.832	
Nidus size			
<3 cm (n=26)	2.74±0.53	2.06±0.64	<0.001*
3–6 cm (n=50)	2.92±0.21	2.65±0.37	<0.001*
>6 cm (n=9)	2.85±0.34	2.37±0.56	0.021*
P value	0.109	<0.001*	
Compactness			
+ (n=70)	2.86±0.35	2.50±0.51	<0. 001*
– (n=15)	2.71±0.38	2.29±0.65	0.042*
P value	0.714	0.037*	

Data are presented as mean ± SD. *, statistical significance. MRA, magnetic resonance angiography; TOF MRA, time-of-flight magnetic resonance angiography; SD, standard deviation.

TOF MRA (1.6±0.7, range, 1–3) than silent MRA (1.8±0.6, range, 1–3) and DSA (1.9±0.6, range, 1–3) (P<0.001). There was no significant difference between the nidus size grading on silent MRA and DSA (P=0.083) (*Figures 5*,*6*). DSA detected 29 deep draining veins. Silent MRA missed five deep draining veins (82.8%, 24/29) detected on DSA, while TOF MRA did not identify seven (75.9%, 22/29) (*Figures 5B*,*6*). DSA detected a total of 18 associated aneurysms, including nine intranidal aneurysms and nine flow-related aneurysms. Silent MRA detected seven intranidal aneurysms (77.8%, 7/9) and all flow-related aneurysms (100%, 9/9). In comparison, TOF MRA detected two intranidal aneurysms (22.2%, 2/9) and seven flow-related aneurysms (77.8%, 7/9) (*Figure 5C*).

The accuracy and comparison of the two MRA techniques in the characterization and Spetzler-Martin grading of BAVMs are shown in *Figure 5* and *Table 3*. In general, the accuracy of silent MRA in nidus size grading and Spetzler-Martin grading was significantly higher than that of TOF MRA (P<0.001). The accuracy of silent MRA in detecting deep venous drainage and associated aneurysms was higher than that of TOF MRA, but the difference was not statistically significant (P=0.402 and 0.098, respectively).

There was no significant difference in the accuracy of silent MRA to detect the BAVM characteristics and perform Spetzler-Martin grading among the various subgroups (P>0.05) (*Table 3*). No interaction was observed among the grouping variables. The accuracy of the TOF MRA in nidus size grading was significantly lower in the medium-size subgroup than the small-size subgroup (P<0.001).

Discussion

This study examined the performance of silent MRA and TOF MRA in the characterization and Spetzler-Martin grading of BAVMs using DSA as the standard. Compared to TOF MRA, silent MRA performed better in terms of image quality, accuracy in determining nidus size, and Spetzler-Martin grading. In addition, the results indicated that the performance of silent MRA was unaffected

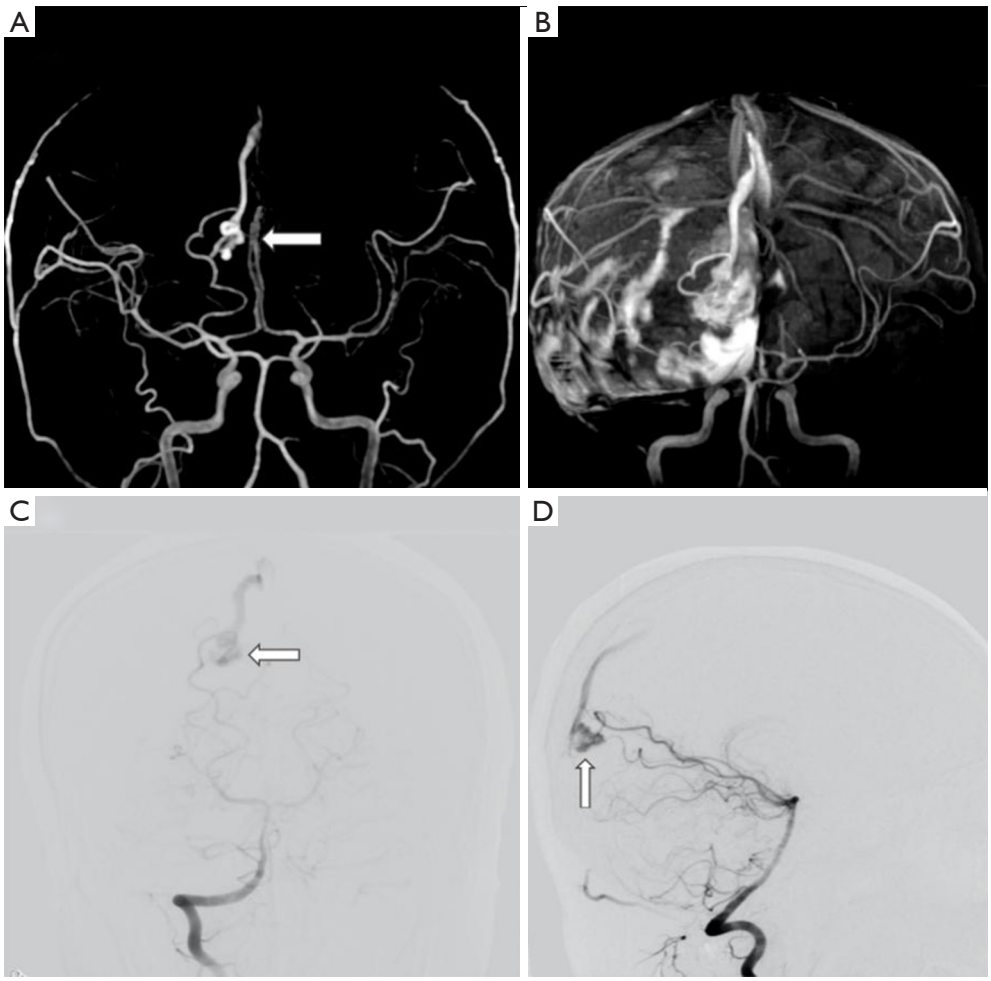

Figure 2 Effects of new hemorrhage on image quality using the two MRA techniques. Images of right occipital lobe BAVM in a 26-year-old man with acute intracranial hemorrhage and diffused subdural hematoma. (A) The feeding artery, nidus, and the draining vein were visible on silent MRA (arrow). The image quality scores are as follows: feeding artery: 3; nidus: 3, and draining vein: 3. (B) TOF MRA exhibited diffused hyperintensity. The feeding artery was invisible, and the nidus and the draining vein were indistinct. The image quality scores are as follows: feeding artery: 0; nidus: 1; and draining vein: 1. (C,D) The front and lateral view of the right vertebral artery angiography showed a small nidus fed by the right posterior cerebral artery (arrows). BAVM, brain arteriovenous malformation; MRA, magnetic resonance angiography; TOF MRA, time-of-flight MRA.

by the presentation of a new hemorrhage, a history of embolization, nidus size, or compactness; thus, silent MRA could be a reliable imaging tool in BAVM evaluation.

Similar to previous studies, our study used 3D MIP images of two MRA techniques for comparison (14,20,21). However, in terms of the study method, our study differed from previous studies in several areas. First, TOF MRA and silent MRA were obtained using the same magnetic field strength and during the same examination in our study, and the spatial resolution of both MRA techniques was the same, which allowed for a more accurate comparison of the two techniques (20,21). Second, subjective scores were employed instead of the signal-noise ratio (SNR) and contrast-to-noise ratio (CNR) to evaluate the image quality. This eliminated the disparity between the image SNR or CNR, and the superiority of BAVM presentation demonstrated in some studies (19). A study based on phantom measurements revealed that conventional SNRs determined based on independent signal and noise regions in a single image do not generally correspond to the true SNR measured in

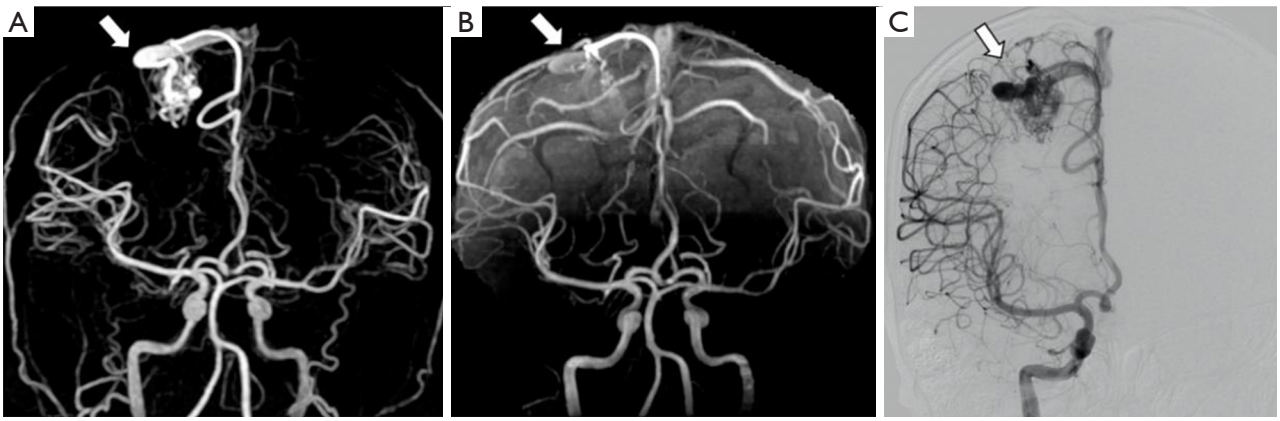

Figure 3 The advantage of depicting small and compact nidus on silent MRA. Images of unruptured and untreated right parietal lobe BAVM in a 23-year-old man. (A) Silent MRA visualized the nidus and draining veins (arrow). The image quality scores are as follows: feeding artery: 3; nidus: 3, and draining vein: 3. (B) The nidus and the draining veins (arrow) were faintly seen on TOF MRA. The image quality scores are as follows: feeding artery: 3; nidus: 2, and draining vein: 2. (C) The front view of the right internal carotid artery angiography showed the nidus and the draining veins (arrow). MRA, magnetic resonance angiography; TOF MRA, time-of-flight MRA.

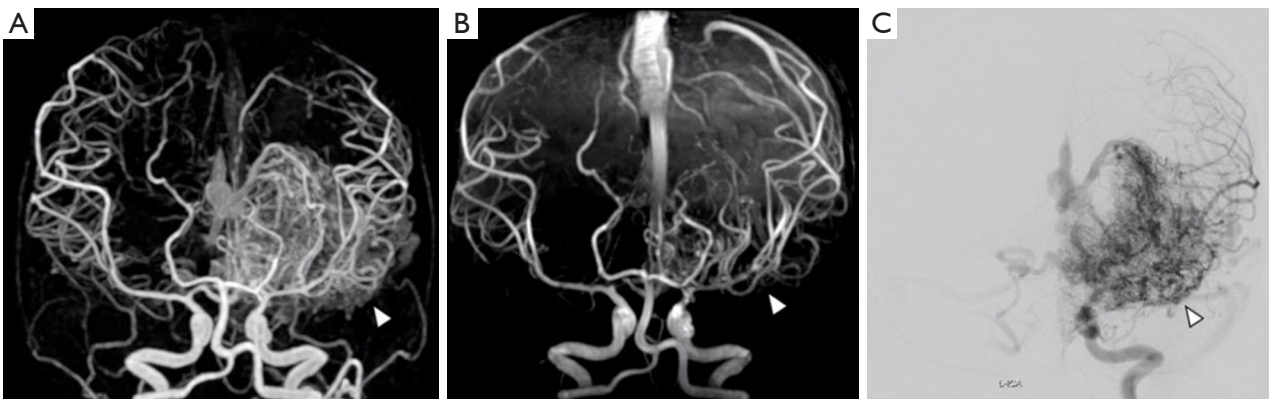

Figure 4 The advantage of depicting diffuse nidus on silent MRA. Images of a giant diffuse BAVM in the left cerebral hemisphere in a 5-year-old girl. (A) Silent MRA visualized the giant nidus (arrowhead). The image quality scores are as follows: feeding artery: 3; nidus: 3, and draining vein: 3. (B) The nidus and the draining veins (arrowhead) were faintly seen on TOF MRA. The image quality scores are as follows: feeding artery: 2; nidus: 1, and draining vein: 2. (C) The front view of the left internal carotid artery angiography showed the nidus (arrowhead). MRA, magnetic resonance angiography; TOF MRA, time-of-flight MRA.

images following the application of reconstruction filters, multichannel reconstruction, or parallel imaging (24). Notably, we divided the sample into a variety of clinically relevant conditions for comparative purposes to validate the usefulness of silent MRA and establish its reliability and its performance in different clinical situations in BAVM imaging.

We found that compared with the gold standard DSA, silent MRA was able to identify all feeding arteries, the nidus, and the vast majority of draining veins, and excelled as a non-invasive ASL-based angiographic sequence in displaying BAVM angioarchitecture. These results are consistent with those reported in previous studies (25,26). In relation to image quality, we found that the overall image quality of silent MRA was significantly superior than that of TOF MRA. The finding of the current study, which

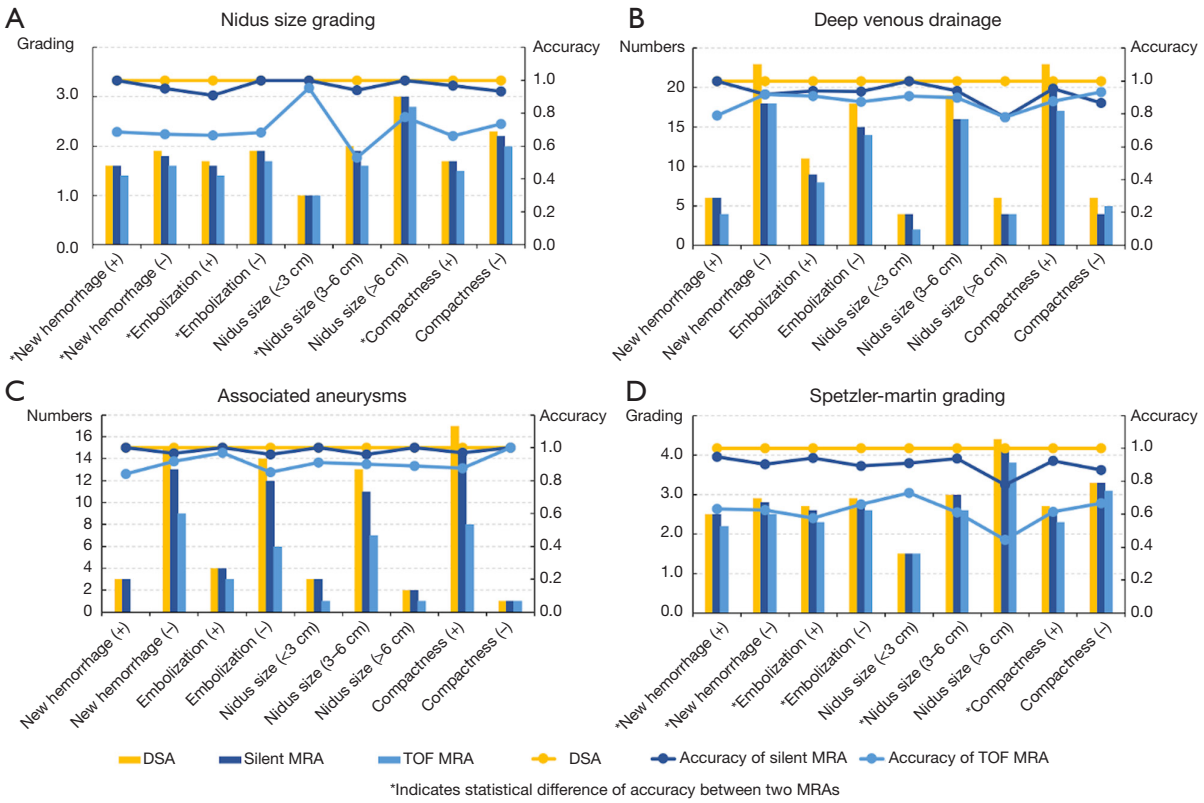

Figure 5 Determination and accuracy of BAVM characteristics on silent MRA and TOF MRA in subgroups. (A) Nidus size grading on silent MRA and TOF MRA. (B) Determination of deep draining veins on silent MRA and TOF MRA. (C) Determination of associated aneurysms on silent MRA and TOF MRA. (D) Spetzler-Martin grading on silent MRA and TOF MRA. BAVM, brain arteriovenous malformation; MRA, magnetic resonance angiography; TOF MRA, time-of-flight MRA.

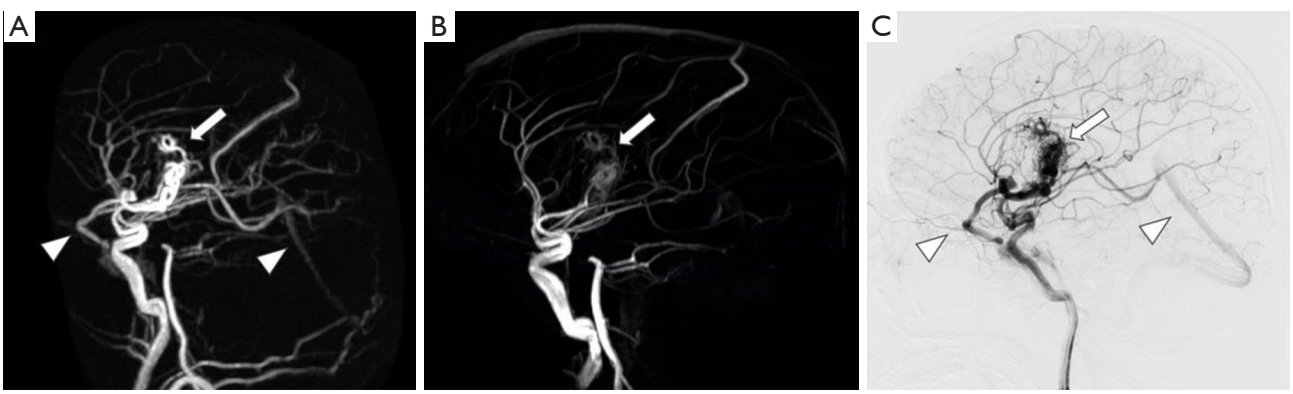

Figure 6 The advantage of depicting partial embolized nidus and draining veins on silent MRA. Images of right temporal lobe BAVM after partial embolization in a 15-year-old male patient. (A) Silent MRA visualized the nidus (thick arrow) and the draining veins (arrowheads). The image quality scores are as follows: feeding artery: 3; nidus: 3; and draining vein: 3. (B) The nidus (thick arrow) was faintly seen on TOF MRA, while the two veins draining downward were not visualized. The image quality scores are as follows: feeding artery: 3; nidus: 2; and draining vein: 0. (C) Lateral view of the right internal carotid artery angiography showed the nidus (thick arrow) with partial embolization draining forward down into the cavernous sinus and back down into the straight sinus (arrowheads). MRA, magnetic resonance angiography; TOF MRA, time-of-flight MRA.

Table 3 Subgroup assessment of accuracy of BAVM characterization and grading on silent MRA and TOF MRA

Subgroup grading criteria	Nidus size grading			Pattern of venous drainage			Associated aneurysm			Spetzler-Martin grading		
	Silent MRA	TOF MRA	P value	Silent MRA	TOF MRA	P value	Silent MRA	TOF MRA	P value	Silent MRA	TOF MRA	P value
Total (n=80)	0.963 (77/80)	0.675 (54/80)	<0.01*	0.938 (75/80)	0.888 (71/80)	0.402	0.975 (78/80)	0.90 (72/80)	0.098	0.913 (73/80)	0.625 (50/80)	<0.01*
New hemorrhage												
+ (n=19)	1 (19/19)	0.684 (13/19)	0.020*	1 (19/19)	0.789 (15/19)	0.105	1 (19/19)	0.842 (16/19)	0.230	0.947 (18/19)	0.632 (12/19)	0.042*
– (n=61)	0.951 (58/61)	0.672 (41/61)	<0.001*	0.918 (56/61)	0.918 (56/61)	1	0.967 (59/61)	0.918 (56/61)	0.439	0.902 (55/61)	0.623 (38/61)	0.001*
P value	0.438	0.579		0.247	0.130		0.579	0.285		0.469	0.585	
Embolization												
+ (n=33)	0.909 (30/33)	0.667 (22/33)	0.033*	0.939 (31/33)	0.909 (30/33)	0.5	1 (33/33)	0.969 (32/33)	0.5	0.939 (31/33)	0/576 (19/33)	0.002*
– (n=47)	1 (47/47)	0.681 (32/47)	<0.001*	0.936 (44/47)	0.872 (41/47)	0.486	0.957 (45/47)	0.851 (40/47)	0.158	0.894 (42/47)	0.660 (31/47)	0.012*
P value	0.066	0.541		0.665	0.446		0.342	0.082		0.386	0.298	
Nidus size												
<3 cm (n=22)	1 (22/22)	0.955 (21/22)	0.5	1 (22/22)	0.909 (20/22)	0.488	1 (22/22)	0.909 (20/22)	0.488	0.909 (20/22)	0.727 (16/22)	0.240
3–6 cm (n=49)	0.939 (46/49)	0.531 (26/49)	<0.001*	0.939 (46/49)	0.898 (44/49)	0.715	0.959 (47/49)	0.898 (44/49)	0.436	0.939 (46/49)	0.612 (30/49)	<0.001*
>6 cm (n=9)	1 (9/9)	0.778 (7/9)	0.471	0.778 (7/9)	0.778 (7/9)	1	1 (9/9)	0.889 (8/9)	0.5	0.778 (7/9)	0.444 (4/9)	0.335
P value	0.373	0.002		0.068	0.538		0.523	0.983		0.290	0.322	
Compactness												
+ (n=65)	0.969 (63/65)	0.662 (43/65)	<0.001*	0.954 (62/65)	0.877 (57/65)	0.206	0.969 (63/65)	0.877 (57/65)	0.096	0.923 (60/65)	0.615 (40/65)	<0.001*
– (n=15)	0.933 (14/15)	0.733 (11/15)	0.330	0.867 (13/15)	0.933 (14/15)	0.5	1 (15/15)	1 (15/15)	1	0.867 (13/15)	0.667 (10/15)	0.390
P value	0.468	0.418		0.234	0.464		0.658	0.174		0.391	0.477	

Values are presented as accuracy rate with the ratio of the accurate number to the total number in parentheses. *, statistical significance. BAVM, brain arteriovenous malformation; MRA, magnetic resonance angiography; TOF MRA, time-of-flight magnetic resonance angiography.

involved a larger sample size, was consistent with previous studies in terms of the image quality assessment (14,20).

A further analysis showed that the image quality of silent MRA was better than that of TOF MRA across all subgroups. This might be due to several factors. First, in silent MRA, inflowing spins are labeled and visualized using distinct sequences. By subtracting the pictures with various labeling sequences, a nearly zero background can be produced. Superior background suppression can help to improve the visualization of each component of BAVM (14). Superior background suppression will have a positive effect on clinical applications of silent MRA. For instance, hemorrhage is the most common symptom of BAVM. New hemorrhage may show high-signal intensity on TOF MRA and significantly alter the display of BAVM components or certain angioarchitecture characteristics. In addition to hemorrhage, Holdsworth *et al.* also found that the application of silent MRA can also improve image readability in the presence of some other T1 high-signal lesions, such as Rathke's cleft cysts or paranasal sinus retention cysts (27). Better background suppression may also result in there being no difference in image quality between diffuse and compact nidus on silent MRA. Second, in addition to better background suppression, silent MRA is substantially less sensitive to the turbulent flow and flow direction, as it uses zTE and accelerated 3D radial acquisition. This represents an advantage over TOF MRA, and the effect is especially noticeable when evaluating draining veins and nidus. On TOF MRA, if the nidus drains downward, the draining vein is difficult to detect because of signal saturation and the absence of an inflow effect. The spin loss caused by complex or turbulent flow in the nidus also affects the display and accurate grading of nidus (14,16,27). Conversely, silent MRA is not affected by turbulence. Thus, it is ideally suited for nidus depiction. This also explains why Spetzler-Martin grading is more accurate on silent MRA, as observed in previous studies and the present research (20,21). Grading is vital for the appropriate selection of candidates for microsurgical procedures. We also showed that the high performance of silent MRA on nidus size and Spetzler-Martin grading was unaffected by embolization, and the size and morphology of the nidus, which has not been reported previously. Given its high performance on nidus visualization and grading, the clinical usage of silent MRA could be expanded, particularly for BAVM follow-up.

Previous studies have closely examined the evaluation of aneurysms on silent MRA, but these studies focused on the visualization of aneurysms after treatment (28-33), and did not examine associated aneurysms of BAVM. In the present study, more associated aneurysms were detected on silent MRA, and the accuracy of silent MRA in the detection of associated aneurysms was higher than that of TOF MRA, but the difference was not statistically significant. However, this might be related to the relatively small number of associated aneurysms in the cohort.

The current study not only revealed the advantages and good performance in different clinical situations of silent MRA in displaying and grading BAVM, but also its limitations in displaying deep venous drainage. Similar to previous research, silent MRA identified more deep draining veins than TOF MRA in this study. Nonetheless, silent MRA was incapable of identifying every deep draining vein. This was also observed in other similar studies on silent MRA (19-21,34). The signal of draining veins obtained on silent MRA depend on the T1 value of the local blood vessel. Because of T1 recovery, the signal decreases with the transit time from the labeling plane (34). Draining veins with different transit times have different amounts of T1 recovery in silent MRA. Wu *et al.* discovered that the absence of draining veins on silent MRA could be the result of signal decay with the blood T1 recovery caused by slow blood flow (22). Prolonging post label delay in silent MRA scanning may aid in resolving this problem, but it would also result in incomplete subtraction and degrade the image quality. To address this issue, further studies are required. Thus, clinicians should be very cautious in using the results of deep draining vein determinations on silent MRA.

Our study had several limitations. First, selection bias was unavoidable, as the data from all patients were evaluated retrospectively. Second, we evaluated the image quality and diagnostic performance of silent MRA in the treatment subgroups. However, our study only included embolization cases. Given that the treatment of BAVMs with radiosurgery or surgical excision after clipping may have various effects on silent MRA and TOF MRA, future studies need to evaluate BAVMs treated with other methods. Third, a small proportion of draining veins were not detected on silent MRA. We hypothesize that this was mainly due to low blood flow velocity. Future studies with larger sample sizes need to investigate whether this is related to the diameter of the draining veins or the image resolution of the sequence. Finally, this study was conducted at a single institution, and multicenter studies need to be conducted to further verify the technique's performance.

Conclusions

Compared to TOF MRA, silent MRA showed good performance in determining nidus size and Spetzler-Martin grading, making it a promising technique for BAVM imaging. However, it should be noted that its ability to detect deep draining veins is limited.

Acknowledgments

Funding: This study was supported by the National Natural Science Foundation of China (No. 82102009 to C.W.; No. 82201439 to J.Y.; No. 82330038 to T.H.; and No. 82220108010 to H.Z.).

Footnote

Reporting Checklist: The authors have completed the STROBE reporting checklist. Available at https://qims.amegroups.com/article/view/10.21037/qims-24-1097/rc

Conflicts of Interest: All authors have completed the ICMJE uniform disclosure form (available at https://qims.amegroups.com/article/view/10.21037/qims-24-1097/coif). The authors have no conflicts of interest to declare.

Ethical Statement: The authors are accountable for all aspects of the work in ensuring that questions related to the accuracy or integrity of any part of the work are appropriately investigated and resolved. The study was conducted in accordance with the Declaration of Helsinki (as revised in 2013). This study was approved by the Ethics Committee of Xuanwu Hospital of Capital Medical University (Xuanwu Hospital, No. 2022079). Informed consent was obtained from all adult patients. For patients under 18 years old, consent was obtained from their parents or legal guardians.

References

1. Fullerton HJ, Achrol AS, Johnston SC, McCulloch CE, Higashida RT, Lawton MT, Sidney S, Young WL; . Long-term hemorrhage risk in children versus adults with brain arteriovenous malformations. Stroke 2005;36:2099-104.
2. Richling B, Killer M, Al-Schameri AR, Ritter L, Agic R, Krenn M. Therapy of brain arteriovenous malformations: multimodality treatment from a balanced standpoint. Neurosurgery 2006;59:S148-57; discussion S3-13.
3. Chen CJ, Ding D, Derdeyn CP, Lanzino G, Friedlander RM, Southerland AM, Lawton MT, Sheehan JP. Brain arteriovenous malformations: A review of natural history, pathobiology, and interventions. Neurology 2020;95:917-27.
4. Ding D, Chen CJ, Starke RM, Kano H, Lee JYK, Mathieu D, Feliciano C, Rodriguez-Mercado R, Almodovar L, Grills IS, Kondziolka D, Barnett GH, Lunsford LD, Sheehan JP. Risk of Brain Arteriovenous Malformation Hemorrhage Before and After Stereotactic Radiosurgery. Stroke 2019;50:1384-91.
5. van Beijnum J, van der Worp HB, Buis DR, Al-Shahi Salman R, Kappelle LJ, Rinkel GJ, van der Sprenkel JW, Vandertop WP, Algra A, Klijn CJ. Treatment of brain arteriovenous malformations: a systematic review and meta-analysis. JAMA 2011;306:2011-9.
6. Spetzler RF, Martin NA. A proposed grading system for arteriovenous malformations. J Neurosurg 1986;65:476-83.
7. Stefani MA, Porter PJ, terBrugge KG, Montanera W, Willinsky RA, Wallace MC. Large and deep brain arteriovenous malformations are associated with risk of future hemorrhage. Stroke 2002;33:1220-4.
8. Stefani MA, Porter PJ, terBrugge KG, Montanera W, Willinsky RA, Wallace MC. Angioarchitectural factors present in brain arteriovenous malformations associated with hemorrhagic presentation. Stroke 2002;33:920-4.
9. Khaw AV, Mohr JP, Sciacca RR, Schumacher HC, Hartmann A, Pile-Spellman J, Mast H, Stapf C. Association of infratentorial brain arteriovenous malformations with hemorrhage at initial presentation. Stroke 2004;35:660-3.
10. Atkinson RP, Awad IA, Batjer HH, Dowd CF, Furlan A, et al. Reporting terminology for brain arteriovenous malformation clinical and radiographic features for use in clinical trials. Stroke 2001;32:1430-42.
11. Illies T, Forkert ND, Saering D, Wenzel K, Ries T,

Regelsberger J, Wegscheider K, Fiehler J. Persistent hemodynamic changes in ruptured brain arteriovenous malformations. Stroke 2012;43:2910-5.
12. Raoult H, Bannier E, Robert B, Barillot C, Schmitt P, Gauvrit JY. Time-resolved spin-labeled MR angiography for the depiction of cerebral arteriovenous malformations: a comparison of techniques. Radiology 2014;271:524-33.
13. Chang W, Loecher MW, Wu Y, Niemann DB, Ciske B, Aagaard-Kienitz B, Kecskemeti S, Johnson KM, Wieben O, Mistretta C, Turski P. Hemodynamic changes in patients with arteriovenous malformations assessed using high-resolution 3D radial phase-contrast MR angiography. AJNR Am J Neuroradiol 2012;33:1565-72.
14. Wu H, Block WF, Turski PA, Mistretta CA, Johnson KM. Noncontrast-enhanced three-dimensional (3D) intracranial MR angiography using pseudocontinuous arterial spin labeling and accelerated 3D radial acquisition. Magn Reson Med 2013;69:708-15.
15. Koktzoglou I, Gupta N, Edelman RR. Nonenhanced extracranial carotid MR angiography using arterial spin labeling: improved performance with pseudocontinuous tagging. J Magn Reson Imaging 2011;34:384-94.
16. Alibek S, Vogel M, Sun W, Winkler D, Baker CA, Burke M, Gloger H. Acoustic noise reduction in MRI using Silent Scan: an initial experience. Diagn Interv Radiol 2014;20:360-3.
17. Hwang ZA, Li CW, Lin CE, Chen JH, Chen CY, Chan WP. Intensity of arterial structure acquired by Silent MRA estimates cerebral blood flow. Insights Imaging 2021;12:185.
18. Zhang Z, Wang Y, Zhou S, Li Z, Peng Y, Gao S, Zhu G, Wu F, Wu B. The automatic evaluation of steno-occlusive changes in time-of-flight magnetic resonance angiography of moyamoya patients using a 3D coordinate attention residual network. Quant Imaging Med Surg 2023;13:1009-22.
19. Tomura N, Saginoya T, Kokubun M, Horiuchi K, Watanabe Z. Comparison of Time-of-Flight-Magnetic Resonance Angiography From Silent Scan Magnetic Resonance Angiography in Depiction of Arteriovenous Malformation of the Brain. J Comput Assist Tomogr 2019;43:943-7.
20. Arai N, Akiyama T, Fujiwara K, Koike K, Takahashi S, Horiguchi T, Jinzaki M, Yoshida K. Silent MRA: arterial spin labeling magnetic resonant angiography with ultra-short time echo assessing cerebral arteriovenous malformation. Neuroradiology 2020;62:455-61.
21. Schubert T, Clark Z, Sandoval-Garcia C, Zea R, Wieben O, Wu H, Turski PA, Johnson KM. Non contrast, Pseudo-Continuous Arterial Spin Labeling and Accelerated 3-Dimensional Radial Acquisition Intracranial 3-Dimensional Magnetic Resonance Angiography for the Detection and Classification of Intracranial Arteriovenous Shunts. Invest Radiol 2018;53:80-6.
22. Wu CX, Zang ZX, Hong T, Dong MQ, Shan Y, Zhao ZL, Hou CB, Lu J. Signal intensity ratio of draining vein on silent MR angiography as an indicator of high-flow arteriovenous shunt in brain arteriovenous malformation. Eur Radiol 2021;31:9252-61.
23. Lawton MT, Kim H, McCulloch CE, Mikhak B, Young WL. A supplementary grading scale for selecting patients with brain arteriovenous malformations for surgery. Neurosurgery 2010;66:702-13; discussion 713.
24. Dietrich O, Raya JG, Reeder SB, Reiser MF, Schoenberg SO. Measurement of signal-to-noise ratios in MR images: influence of multichannel coils, parallel imaging, and reconstruction filters. J Magn Reson Imaging 2007;26:375-85.
25. De Simone M, Fontanella MM, Choucha A, Schaller K, Machi P, Lanzino G, Bijlenga P, Kurz FT, Lövblad KO, De Maria L. Current and Future Applications of Arterial Spin Labeling MRI in Cerebral Arteriovenous Malformations. Biomedicines 2024;12:753.
26. Ramachandran S, Mukherjee D, Delf J, Bown MJ, Kandiyil N. A comparison of arterial spin labelling with catheter angiography in evaluating arteriovenous malformations: a systematic review. Br J Radiol 2020;93:20190830.
27. Holdsworth SJ, Macpherson SJ, Yeom KW, Wintermark M, Zaharchuk G. Clinical Evaluation of Silent T1-Weighted MRI and Silent MR Angiography of the Brain. AJR Am J Roentgenol 2018;210:404-11.
28. Ryu KH, Baek HJ, Moon JI, Choi BH, Park SE, Ha JY, Park H, Kim SS, Kim JS, Cho SB, Carl M. Usefulness of Noncontrast-Enhanced Silent Magnetic Resonance Angiography (MRA) for Treated Intracranial Aneurysm Follow-up in Comparison with Time-of-Flight MRA. Neurosurgery 2020;87:220-8.
29. Oishi H, Fujii T, Suzuki M, Takano N, Teranishi K, Yatomi K, Kitamura T, Yamamoto M, Aoki S, Arai H. Usefulness of Silent MR Angiography for Intracranial Aneurysms Treated with a Flow-Diverter Device. AJNR Am J Neuroradiol 2019;40:808-14.
30. Satoh T, Hishikawa T, Hiramatsu M, Sugiu K, Date I. Visualization of Aneurysmal Neck and Dome after Coiling with 3D Multifusion Imaging of Silent MRA and FSE-MR Cisternography. AJNR Am J Neuroradiol 2019;40:802-7.

31. Shang S, Ye J, Dou W, Luo X, Qu J, Zhu Q, Zhang H, Wu J. Validation of Zero TE-MRA in the Characterization of Cerebrovascular Diseases: A Feasibility Study. AJNR Am J Neuroradiol 2019;40:1484-90.
32. Tan S, Lu Y, Li B, Yang Q, Zhou X, Wang Y. Diagnostic performance of silent magnetic resonance angiography for endovascularly-treated intracranial aneurysm follow-up: a prospective study. J Neurointerv Surg 2023;15:608-13.
33. Kim YN, Choi JW, Lim YC, Song J, Park JH, Jung WS. Usefulness of Silent MRA for Evaluation of Aneurysm after Stent-Assisted Coil Embolization. Korean J Radiol 2022;23:246-55.
34. Fujiwara Y, Muranaka Y. Improvement in visualization of carotid artery uniformity using silent magnetic resonance angiography. Radiol Phys Technol 2017;10:113-20.

Cite this article as: Wu C, Dong M, Zang Z, Shan Y, Yu J, Hong T, Yang K, Zhao C, Zhang H, Lu J. Comparison of silent MRA and time-of-flight MRA in the depiction and grading of brain arteriovenous malformations. Quant Imaging Med Surg 2024;14(12):8974-8987. doi: 10.21037/qims-24-1097

